A Battery-Free Wireless EEG Transmission System Using Compressed Sensing and Powered by Body–Ambient Temperature Difference: Outdoor Demonstration at Expo 2025

Daisuke Kanemoto*, Kazane Yoshimoto, Shodai Motomochi, and Tetsuya Hirose
Graduate School of Engineering, The University of Osaka, Suita, Japan
*contact@kanemoto.tech

***Abstract*—The sustainability of wearable sensing devices requires low-power operation. This study presents a battery-free wireless electroencephalography (EEG) transmission system powered solely by energy harvested via a thermoelectric generator. The system integrates compressed sensing (CS) with random undersampling and a waveform-similarity-based reconstruction basis, achieving a high compression ratio (CR) while preserving reconstruction accuracy. An outdoor demonstration at the Expo 2025 site in Osaka, Kansai, Japan confirmed stable on-device operation, including EEG digitization, compression, and wireless transmission, powered by the temperature difference between the body and the ambient air, with the ambient air temperature at 32.5–$32.8\,^{\circ}\mathrm{C}$, without forced airflow or external power. Using 100 segments from the CHB-MIT dataset (chb14), the proposed system was evaluated using a single fixed measurement matrix under the ambient temperature during the demonstration, yielding an average normalized mean square error of 0.047 with $\mathrm{CR} = 6$. These results demonstrate the potential of CS as a next-generation battery-free biosensing platform.**

***Index Terms*—battery-free systems, compressed sensing, Expo 2025 demonstration, low-power systems, random undersampling, thermoelectric energy harvesting, waveform similarity, wireless EEG transmission.**

I. Introduction

Digital transformation (DX) is driving rapid changes across industries, public services, and daily life and is now recognized as a key trend in information and communication technologies [1]. To sustain this shift, society requires sensing infrastructures capable of continuously collecting reliable real-world information and integrating it through connected networks. As a result, internet of things (IoT)-oriented sensor systems must achieve higher performance with substantially reduced power consumption, while also incorporating new power-supply mechanisms that enable long-term autonomous operation.

In wearable sensing applications, such as electroencephalography (EEG), where signals must be continuously monitored over extended periods, reducing the power across the entire signal chain, from the analog front-end to analog-to-digital (A/D) conversion and wireless communication, is essential. However, device-level power reduction through semiconductor scaling is approaching its physical limits, and further miniaturization or voltage scaling alone is no longer sufficient for persistent operation [2]. These constraints motivate a hardware–algorithm co-design strategy in which circuits and signal processing are jointly optimized rather than independently improved [3].

Compressed sensing (CS) [4] exploits sparsity in signals to enable reconstruction from a reduced number of samples. To achieve low-power sensing, we have applied this concept and developed CS-based architectures. In particular, random undersampling is highly suitable for hardware implementation because it reduces both the number of sampling operations and the wireless data volume without significantly degrading the signal fidelity. Previous studies have validated this concept through a combination of numerical simulations, circuit-level designs, and system-level demonstrations across A/D converters (ADCs) [5], low-noise amplifiers [6]–[8], and wireless sensor systems [9]. Although non-uniform sampling—represented by random undersampling—differs from conventional uniform sampling, numerous studies have shown that it can be applied to various sensing scenarios and can achieve efficient compression (e.g., [10]).

A remaining challenge is that the accuracy of CS reconstruction strongly depends on the signal sparsity, whereas biosignals exhibit temporal variations and subject-specific characteristics that often deviate from those of simple sparse models. To address this issue, we previously proposed reconstruction methods that generate bases from past waveform data and exploit waveform similarity to improve accuracy [11]. By leveraging this waveform-similarity-based reconstruction approach, high reconstruction fidelity was maintained even under high compression, thereby enabling an EEG acquisition and wireless transmission system operating with low power consumption [12].

Building on this achievement in low-power operation, this study aims to further demonstrate a fully battery-free wireless EEG transmission system powered solely by the small amount of thermal energy harvested from the temperature difference between the human body and ambient air. By combining CS-based random undersampling with a thermoelectric generator (TEG), the system reduces the number of sampling operations

and transmission power while preserving reconstruction fidelity, enabling complete EEG digitization and communication using only a small amount of harvested thermal energy.

To assess the feasibility of the chosen approach, an outdoor demonstration was conducted at the Expo 2025 site in Osaka, Kansai, Japan. In this experiment, the entire system operated exclusively on body–ambient thermal energy. Even in outdoor conditions, the system successfully performed EEG digitization, compression, and wireless transmission using only the harvested thermal energy, thereby confirming the real-world viability of the proposed battery-free CS-based EEG platform. While our preliminary technical report [13] presented an overview, this paper presents new quantitative results, provides further details of the TEG-based power generation, and discusses the reconstruction accuracy and performance under temperature variations.

The remainder of this paper is organized as follows. Section II describes the CS framework with random undersampling and the waveform-similarity-based reconstruction method. Section III presents the demonstration setup and experimental results. Finally, section IV provides the conclusions.

II. Compressed Sensing with Random Undersampling and Similarity-Based Reconstruction

A. Basics of Compressed Sensing

First, a brief overview of the principle of compressed sensing is provided. Let $\mathbf{x} \in \mathbb{R}^N$ be a vector representing a signal obtained from an observation target where each element corresponds to the sampled signal voltage acquired at uniform time intervals of Δt s. The compressed measurement vector $\mathbf{y} \in \mathbb{R}^M$ is expressed using the measurement matrix $\mathbf{\Phi} \in \mathbb{R}^{M \times N}$ as follows:

$$\mathbf{y} = \mathbf{\Phi}\mathbf{x}. \tag{1}$$

When $M < N$, the number of elements in $\mathbf{y}$ is less than that of $\mathbf{x}$, indicating that the signal is compressed. By defining the compression ratio (CR) as $\mathrm{CR} = N/M$, the value of $\mathrm{CR} = 6$ implies that the data size of $\mathbf{y}$ is reduced to one-sixth of that of $\mathbf{x}$. As $\mathbf{\Phi}$ becomes a wide matrix under the condition $M < N$, the inverse does not exist and the direct reconstruction of $\mathbf{x}$ from $\mathbf{y}$ is generally ill posed. The key to solving this problem in CS lies in exploiting the sparsity inherent in the original signal $\mathbf{x}$.

It is assumed that the signal $\mathbf{x}$ can be represented using a basis matrix $\mathbf{\Psi} \in \mathbb{R}^{N \times P}$ and a sparse vector $\mathbf{s} \in \mathbb{R}^P$ where several elements are zero. Under this assumption, $\mathbf{x}$ can be written as follows:

$$\mathbf{x} = \mathbf{\Psi}\mathbf{s}. \tag{2}$$

However, this representation does not always hold true for an arbitrary signal $\mathbf{x}$. However, for signals such as EEG, which can be approximated as the superposition of periodic components (for example α- and β-band activities), (2) is often approximately satisfied by choosing $\mathbf{\Psi}$ as the inverse Fourier transform or an inverse discrete cosine transform matrix. Furthermore, as discussed in Section II-C, it is possible to generate an appropriate basis $\mathbf{\Psi}$ using a set of previously acquired signals, enabling $\mathbf{x}$ to be represented sparsely. In such cases, the assumption in (2) becomes more reasonable. Under this assumption, there exists a basis in which $\mathbf{x}$ admits a sparse representation.

Combining (1) and (2), the fundamental equation of compressed sensing is as follows:

$$\mathbf{y} = \mathbf{\Phi}\mathbf{x} = \mathbf{\Phi}\mathbf{\Psi}\mathbf{s}. \tag{3}$$

Equation (3) indicates that the measurement vector $\mathbf{y}$ is obtained by mapping an unknown sparse vector $\mathbf{s}$ by using a known matrix $\mathbf{\Phi}\mathbf{\Psi}$. Thus, the reconstruction problem of CS is reduced to estimating the sparsest vector $\mathbf{s}$ that satisfies the measurement constraint. This can be formulated as follows:

$$\hat{\mathbf{s}} = \arg\min_{\mathbf{s}} \|\mathbf{s}\|_0 \quad \text{subject to} \quad \mathbf{y} = \mathbf{\Phi}\mathbf{\Psi}\mathbf{s}, \tag{4}$$

where $\|\cdot\|_0$ denotes the ℓ_0-norm that counts the number of non-zero entries in the vector. This problem seeks the sparsest solution that satisfies the measurement constraint; however, ℓ_0 minimization is NP-hard [14]. Therefore, practical systems employ approximate algorithms with significantly lower computational complexity. Once the sparse vector $\hat{\mathbf{s}}$ is estimated using one of these algorithms, the reconstructed signal $\hat{\mathbf{x}}$ is obtained as follows:

$$\hat{\mathbf{x}} = \mathbf{\Psi}\hat{\mathbf{s}}. \tag{5}$$

This concludes the overview of CS–based sensing systems. The next subsection discusses the design of $\mathbf{\Phi}$, which is critical to sensor-side hardware implementation, and the following subsection discusses basis generation that exploits waveform similarity for high-fidelity reconstruction.

B. Random Undersampling for Low-Power Compression

Compression methods can be categorized as analog-domain (e.g., [15]), digital-domain (e.g., [16]), and random undersampling approaches. The analog approach requires dedicated analog circuitry to perform the matrix–vector multiplication in (1). In the digital approach, computations are performed in the digital domain, yielding high numerical accuracy but requiring a high-speed ADC to sample all the data points.

By contrast, random undersampling compresses using a sensing matrix $\mathbf{\Phi}_{\mathrm{RUS}}$ defined as follows:

$$\mathbf{\Phi}_{\mathrm{RUS}} = \begin{bmatrix} 0 & 1 & 0 & 0 & 0 & \cdots & 0 \\ 0 & 0 & 1 & 0 & 0 & \cdots & 0 \\ 0 & 0 & 0 & 0 & 1 & \cdots & 0 \\ \vdots & \vdots & \vdots & \ddots & \vdots & & \vdots \\ 0 & 0 & 0 & 0 & 0 & \cdots & 1 \end{bmatrix}. \tag{6}$$

Each row of $\mathbf{\Phi}_{\mathrm{RUS}}$ contains exactly one “1”, and the column index of the “1” in successive rows increases monotonically, where the intervals are determined pseudo-randomly. Using $\mathbf{\Phi}_{\mathrm{RUS}}$, simple compression can be performed by skipping samples according to the pattern of “1” entries;

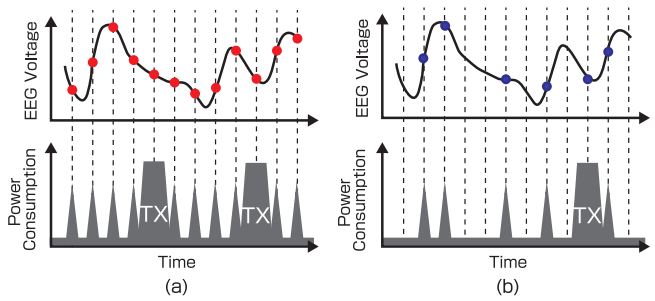

Fig. 1. Illustrations of (a) uniform sampling and (b) random undersampling, showing their sampling behavior and associated power consumption. Random undersampling reduces both sampling events and wireless transmissions, leading to lower power consumption.

no additional analog circuitry, and only a low-speed ADC is required. A conceptual illustration of random undersampling and its power consumption is shown in Fig. 1. This method reduces both the number of sampling events and wireless transmissions, achieving substantial power savings without introducing additional computational overheads.

C. Basis Generation Exploiting Waveform Similarity

As discussed in Section II.B, the design of a basis that enables sparse representation is crucial for improving the reconstruction accuracy and to achieve high compression ratios. While basis design has been explored from multiple perspectives (e.g., [17]), this study adopts an approach that leverages two signal characteristics: (i) natural signals often exhibit strong correlations between current and previously acquired signals [18], and (ii) biosignals such as EEG typically exhibit block or group structures in their representation [19]. Based on these insights, a basis-generation method was developed that exploits waveform similarity. This study uses an EEG-specific basis $\mathbf{\Psi}_{\mathrm{EEG}}$, as proposed by [12], which is constructed by sorting previously acquired EEG segments based on their mean frequency characteristics.

III. Experimental Verification at Expo 2025

This study implemented the system configuration shown in Fig. 2 and experimentally verified its feasibility. EEG test signals were generated by amplifying pre-recorded EEG data to an amplitude suitable for the input range of the ADC and were output using PXIe-4463 (National Instruments). Random undersampling and wireless transmission were performed using the microcontroller-equipped module nRF52840 Dongle (Nordic Semiconductor). The module was powered solely by thermal energy harvested from the temperature difference between the human body and ambient air: a TEG converted the thermal gradient into electrical power, which was then boosted to $3.3\,\mathrm{V}$ using a DC-DC converter LTC3109 (Analog Devices, Inc.). Thus, no external regulated power supply was used and the system operated in a completely battery-free manner. On the receiver side, the compressed data were received via a nRF52840 DK (Nordic Semiconductor), and waveform reconstruction was performed using a PXIe-8861 (National Instruments).

For the EEG test data, the FP1–F7 channel signals from subject chb14 in the CHB–MIT scalp EEG database [20] were used, excluding the segments that correspond to seizure activity. Each segment had a duration of $3\,\mathrm{s}$. The original $256\,\mathrm{Hz}$ sampling rate was resampled to $200\,\mathrm{Hz}$ for evaluation. For all segments, DC components were removed, and segments with absolute amplitudes exceeding $150\,\mu\mathrm{V}$ were regarded as containing artifacts and excluded. After A/D conversion, packets were formed in the data formatting block, and wireless transmission was performed using Bluetooth low energy (BLE) 5. Random undersampling was applied during A/D sampling using a single fixed measurement matrix, $\mathbf{\Phi}_{\mathrm{RUS}}$. In this experiment, CR was set to 6. The ADC resolution was $12\,\mathrm{bits}$ and bit-packing was implemented in the data formatting block to match the available byte size per BLE packet. The dongle was powered exclusively by the energy generated from the temperature difference.

Figure 3(a) shows the power-generation unit, where electrical power is produced by applying the temperature difference between body heat and ambient air to the TEGs. In this setup, eight TG12-8-01LS TEG modules (Marlow Industries, Inc.) were prepared, each equipped with a graphite sheet WW-T68A-14070 (Taiyo Co., Ltd.), and placed on a heat sink. Four modules were connected in series, and two series strings were connected in parallel to form a generation unit. A single copper plate ($10\,\mathrm{cm} \times 20\,\mathrm{cm} \times 2\,\mathrm{mm}$) was placed over each of the four TEGs and fixed in position using clamps, as shown in Fig. 3(b). To generate electrical power, a temperature gradient was applied to the TEGs by placing a hand on the copper plate. Heat was transferred from the hand to the TEG via the copper plate, and all power was generated solely from the temperature difference between the body and the ambient environment. The ambient temperature was measured using a digital temperature data logger AD-5326TT (A&D Company, Ltd.).

The same microcontroller-equipped module nRF52840 DK was used on the receiver side as a transmitter for bit-unpacking. Waveform reconstruction was performed using the PXIe-8861 as a PC platform. Reconstruction employed the matrix $\mathbf{\Phi}_{\mathrm{RUS}}$ and the similarity-based EEG basis $\mathbf{\Psi}_{\mathrm{EEG}}$, using the Block Sparse Bayesian Learning (BSBL)-BO algorithm [21] implemented in Python 3 to obtain the reconstructed waveform $\hat{\mathbf{x}}$.

The demonstration was conducted as a public experiment at the "TEAM EXPO Pavilion" during Expo 2025 in Osaka, Kansai, Japan on September 15. The system is shown in Fig. 4. Although a fan is visible in the photograph, the results reported here were obtained without forced airflow. One example of the operational results of the system is shown in Fig. 5. This result shows an example waveform obtained at an ambient air temperature of $32.5,^{\circ}\,\mathrm{C}$, indicating that accurate waveform reconstruction is achievable even with a fully battery-free system.

In this paper, the reconstruction accuracy is evaluated by introducing the normalized mean square error (NMSE) as a

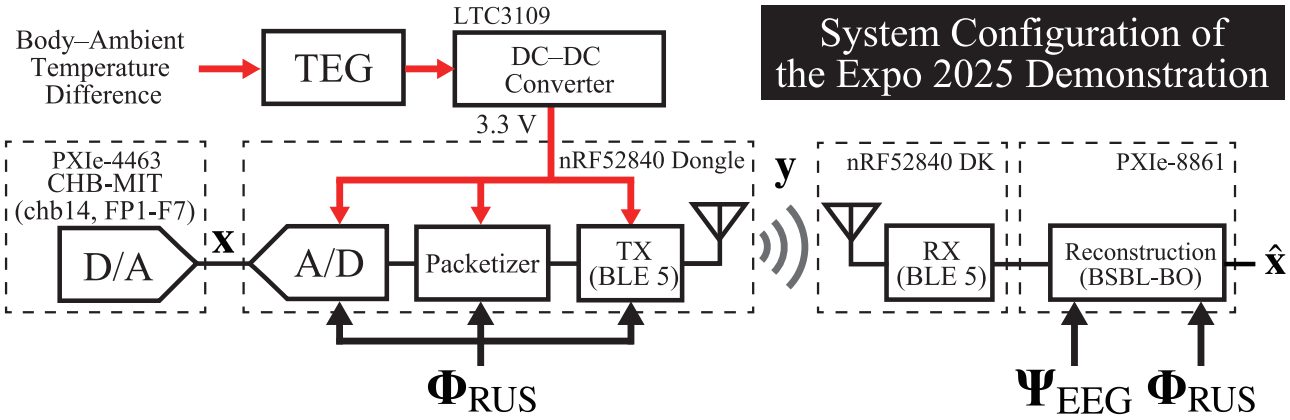

Fig. 2. System block diagram used for verification. The microcontroller on the transmitter side compresses the signal, while the PC on the receiver side reconstructs it. Both share the measurement matrix $\mathbf{\Phi}_{\mathrm{RUS}}$, and the receiver performs signal reconstruction using the basis matrix $\mathbf{\Psi}_{\mathrm{EEG}}$ that was created in advance.

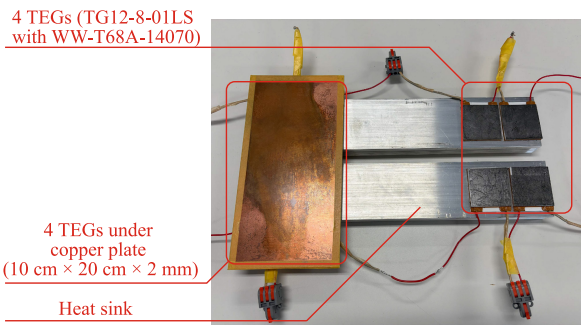

(a) Configuration of the TEG system

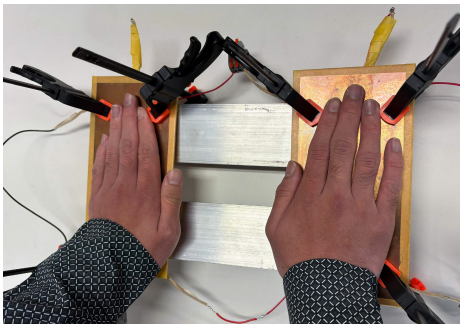

(b) Power generation by placing a hand on the copper plate

Fig. 3. (a) TEGs used in the demonstration. Eight TEG modules were employed, where four modules were connected in series and the two series strings were connected in parallel. A graphite sheet was placed on top of each TEG and a copper plate was positioned above it. (b) Power generation by placing a hand on the copper plate, utilizing the temperature difference between body heat and the ambient air.

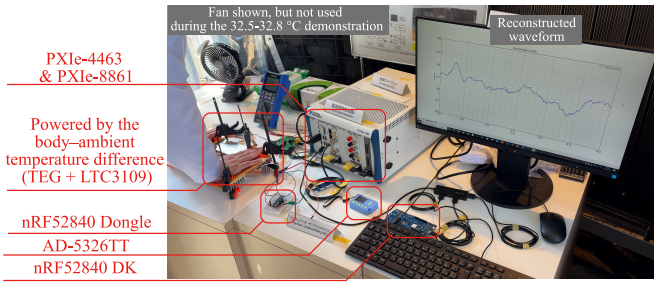

Fig. 4. Photograph of the system that demonstrated battery-free wireless EEG transmission powered solely by the temperature difference between the human body and ambient air at the Expo 2025 site in Osaka, Kansai, Japan.

qualitative metric. The NMSE is defined as

$$\mathrm{NMSE} = \frac{\|\mathbf{x} - \hat{\mathbf{x}}\|_2^2}{\|\mathbf{x}\|_2^2}. \tag{7}$$

Fig. 6 shows the NMSE for the 100-segment case at an ambient temperature of 32.5–32.8 °C. The results shown in the figure are based on 100 segments, each 3 s long, acquired intermittently within the overall measurement window of 10:52—11:04. It can be seen that the NMSE does not change significantly. Moreover, because the chb14 dataset was streamed continuously, the waveform varied across segments; thus, some fluctuation in the NMSE is not uncommon. The average NMSE over these 100 segments was 0.047. The NMSE varies depending on the configuration of the measurement matrix $\mathbf{\Phi}_{\mathrm{RUS}}$ and the characteristics of the target signal. In this study, due to experimental constraints, we evaluated the system using only a single test dataset and a single measurement matrix; therefore, the resulting NMSE may appear slightly better than in a more general setting. Thus, averaging the results over more segments—across multiple measurement matrices and diverse target signals—could yield less biased results. On the other hand, the primary objective of this experiment was to demonstrate that the proposed system can operate solely on power harvested via thermoelectric generation driven by the temperature difference between the body and ambient air, and this objective has been achieved. These results indicate that the proposed system maintained stable operation using only thermoelectrically harvested power even at elevated ambient

TABLE I
COMPARISON OF WIRELESS EEG MEASUREMENT AND TRANSMISSION SYSTEMS OPERATING WITH ENERGY HARVESTERS.

	This work	T. Miyata et al. [9]	T.Torfs et al. [22][(2)]	A.Dementyev et al. [23][(2)]
Energy harvester	**TEG**	TEG	TEG	Wireless power transfer
Power generation conditions	**Body vs. ambient temperature difference (ambient** $32.5 - 32.8\,^{\circ}\mathrm{C}$**)**[(1)]	Artificially-generated $2\,^{\circ}\mathrm{C}$ temperature difference[(1)]	Body–ambient temperature difference (ambient 22–23 °C)	Stable operation within $\approx 0.8\,\mathrm{m}$ of the antenna
CR	**6**	4	N/A	N/A
Reconstruction algorithm, basis	**BSBL-BO,** $\boldsymbol{\Psi}_{\mathrm{EEG}}$	OMP, DCT	N/A	N/A
NMSE	**0.047** [(3)]	0.24	N/A	N/A

[(1)] No forced airflow by fan [(2)] with analog EEG amplification circuitry
[(3)] Our NMSE is obtained using a single dataset (chb14) and a single measurement matrix; the primary goal of this work is energy-autonomous operation.

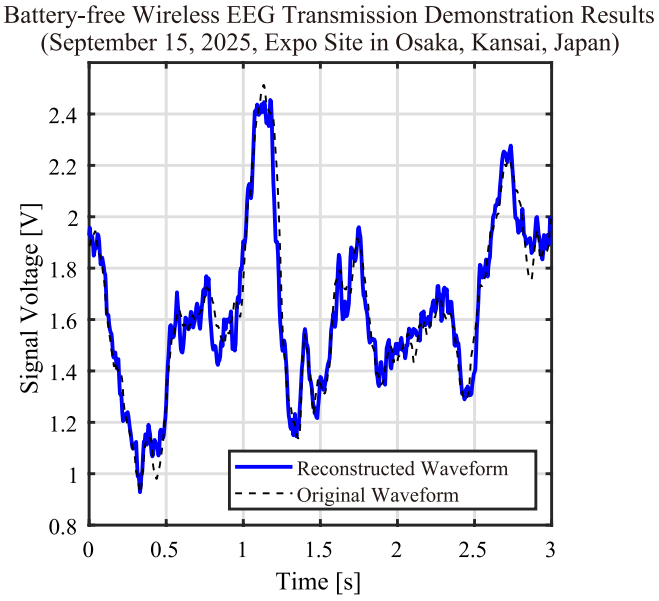

Fig. 5. Waveform reconstructed using power generated solely from the temperature difference between the human body and ambient air ($32.5\,^{\circ}\mathrm{C}$). The EEG input voltage was preprocessed and adjusted to fully utilize the ADC full-scale range. The compression ratio was $\mathrm{CR} = 6$, thereby confirming battery-free operation and demonstrating high reconstruction accuracy.

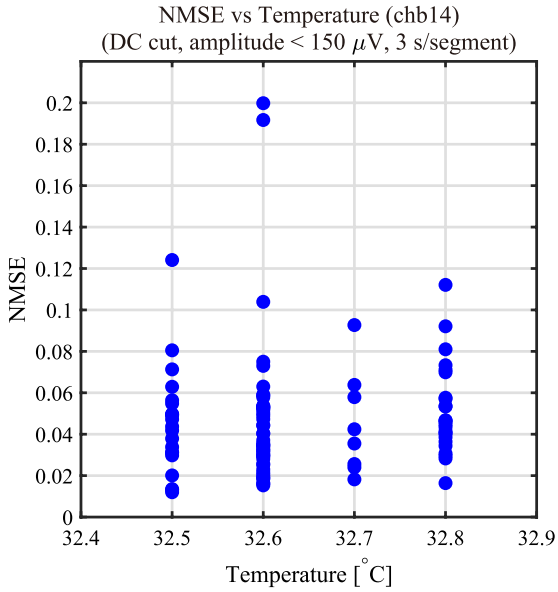

Fig. 6. NMSE over 100 segments acquired intermittently between 10:52 and 11:04 at an ambient air temperature of 32.5–32.8°C. The system operated solely on thermoelectrically harvested power while streaming 100 segments from the chb14 dataset using a single fixed measurement matrix (average NMSE: 0.047).

air temperatures (32.5–$32.8\,^{\circ}\mathrm{C}$), enabling wireless EEG transmission without any external power source.

Table I summarizes wireless EEG systems powered by energy harvesters, including the system demonstrated in this work. [9] and [22] use TEGs similar to that employed in this study. In [9], system operation was confirmed using the power generated from a temperature difference of only $2\,^{\circ}\mathrm{C}$; however, the evaluation was conducted under artificially stabilized thermal conditions. In [22] the total system power consumption was approximately $0.8\,\mathrm{mW}$, and the evaluation was limited to room-temperature conditions (22–$23\,^{\circ}\mathrm{C}$), without reporting operation in high-temperature environments where the ambient temperature approaches body temperature. Meanwhile, [23] demonstrated system operation using RF energy harvesting in the UHF band (902–928 MHz). However, owing to link budget limitations, stable operation was achievable only within approximately $0.8\,\mathrm{m}$ of the power-transmitting antenna.

The proposed system successfully achieved wireless EEG transmission in a high-temperature outdoor environment at an ambient air temperature of 32.5–$32.8\,^{\circ}\mathrm{C}$, using only a small amount of thermal energy harvested by the TEG from the body–ambient air temperature difference. Moreover, because the system is powered by TEG-based energy harvesting, it imposes no distance constraints on power generation. This result was enabled by random undersampling-based signal acquisition, which significantly reduced the transmission data volume and power consumption, and by waveform-similarity-based basis generation, which maintained high reconstruction accuracy even under high compression. Therefore, the developed system provides an effective low-power sensing architecture that enables practical battery-free wireless EEG

transmission powered solely by naturally occurring body–ambient air thermal energy, without external power sources or forced thermal management.

IV. CONCLUSION

This study explained a low-power wireless EEG transmission system based on CS and achieved fully self-powered operation using a thermoelectric energy harvester. By reducing both the sampling operations and the transmitted data volume via random undersampling, while preserving reconstruction accuracy through BSBL-BO with waveform-similarity-based basis generation, substantial power savings were achieved without compromising signal fidelity. Stable battery-free operation, including EEG digitization, compression, and wireless transmission, was confirmed in an outdoor demonstration at the Expo 2025 site in Osaka, Kansai, Japan at an ambient temperature of 32.5–$32.8\,^{\circ}\mathrm{C}$ without forced airflow or external power. Furthermore, using 100 segments from the chb14 dataset, the reconstruction performance was evaluated using only a single fixed measurement matrix, yielding an average NMSE of 0.047. These results validate CS-based signal-processing and hardware co-design and support energy-harvester-driven architectures as a promising approach for next-generation low-power wearable sensing systems.

ACKNOWLEDGMENT

This work was supported by JSPS KAKENHI Grant Number JP24K02914. This paper is based on results obtained from a project,JPNP14004, commissioned by the New Energy and Industrial Technology Development Organization (NEDO).

REFERENCES

[1] U. Ahrend, M. Aleksy, M. Berning, J. Gebhardt, F. Mendoza, and D. Schulz, "Sensors as the basis for digitalization: New approaches in instrumentation, IoT–concepts, and 5G," *Internet Things*, vol. 15, pp. 1–16, Sep. 2021, doi: 10.1016/j.iot.2021.100406.

[2] H.-S. Ku, S. Choi, and J.-Y. Sim, "A $12\,\mu$s-conversion, $20\,\mathrm{m}$K-resolution temperature sensor based on SAR ADC," *IEEE J. Solid-State Circuits Syst. II, Exp. Briefs*, vol. 69, no. 3, pp. 789–793, Mar. 2021, doi: 10.1109/TCSII.2021.3107899.

[3] D. Kanemoto, "Technical note—slowdown in the energy efficiency of analog-to-digital converters and a compressed-sensing-based solution," The University of Osaka Institutional Knowledge Archive (OUKA), Tech. Note, Jun. 2025, doi: 10.18910/101986.

[4] D. L. Donoho, "Compressed sensing," *IEEE Trans. Inf. Theory*, vol. 52, no. 4, pp. 1289–1306, Apr. 2006, doi: 10.1109/TIT.2006.871582.

[5] Y. Okabe, D. Kanemoto, O. Maida, and T. Hirose, "Compressed sensing EEG measurement technique with normally distributed sampling series," *IEICE Trans. Fundamentals*, vol. E105-A, no. 10, pp. 1429–1433, Oct. 2022, doi: 10.1587/transfun.2021EAL2099.

[6] K. Mii, D. Kanemoto, and T. Hirose, "$0.36\,\mu$W/channel capacitively-coupled chopper instrumentation amplifier in EEG recording wearable devices for compressed sensing framework," *Jpn. J. Appl. Phys.*, vol. 63,03SP54, 2024, doi: 10.35848/1347-4065/ad264f.

[7] R. Matsubara, D. Kanemoto, and T. Hirose, "Reducing power consumption in LNA by utilizing EEG signals as basis matrix in compressed sensing," in *Proc. IEEE Int. Symp. Circuits Syst. (ISCAS)*, May 2024, pp. 1–5, doi: 10.1109/ISCAS58744.2024.10558519.

[8] R. Matsubara, D. Kanemoto, and T. Hirose, "Design guidelines for noise in a low-noise amplifier using EEG signals as a basis matrix in compressed sensing system," in *Proc. IEEE Int. Conf. Consum. Electron. (ICCE)*, Jan. 2025, pp. 1–5, doi: 10.1109/ICCE63647.2025.10930098.

[9] T. Miyata, D. Kanemoto, and T. Hirose, "Random undersampling wireless EEG measurement device using a small TEG," in *Proc. IEEE Int. Symp. Circuits Syst. (ISCAS)*, May 2023, pp. 1–5, doi: 10.1109/ISCAS46773.2023.10181822.

[10] R. Tsunaga, D. Kanemoto, and T. Hirose, "Noise-masking cryptosystem using watermark and chain generation for EEG measurement with compressed sensing," in *Proc. IEEE Int. Conf. Consum. Electron. (ICCE)*, Jan. 2024, pp. 1–6, doi: 10.1109/ICCE59016.2024.10444172.

[11] D. Kanemoto and T. Hirose, "EEG measurements with compressed sensing utilizing EEG signals as the basis matrix," in *Proc. IEEE Int. Symp. Circuits Syst. (ISCAS)*, May 2023, pp. 1–5, doi: 10.1109/ISCAS46773.2023.10181710.

[12] D. Kanemoto, E. Takimoto, and T. Hirose, "Development of low-power and high-accuracy wireless EEG transmission system using compressed sensing with an EEG basis," in *Proc. IEEE Int. Symp. Circuits Syst. (ISCAS)*, May 2025, pp. 1–5, doi: 10.1109/ISCAS56072.2025.11043415.

[13] D. Kanemoto, K.Yoshimoto, S.Motomochi, and T. Hirose, "A low-power wireless EEG transmission system with hardware-signal processing integration using compressed sensing – outdoor verification at the Expo site: Operation with only minimal energy harvested from body-ambient temperature differences –," in *IEICE Tech. Rep.*, Dec. 2023, pp. 117–122, (in Japanese).

[14] B. K. Natarajan, "Sparse approximate solutions to linear systems," *SIAM J. Comput.*, vol. 24, no. 2, pp. 227–234, Apr. 1995, doi: 10.1137/S0097539792240406.

[15] X. Chen, Z. Yu, S. Hoyos, B. M. Sadler, and J. Silva-Martinez, "A sub-nyquist rate sampling receiver exploiting compressive sensing," *IEEE Trans. Circuits Syst. I, Reg. Papers*, vol. 58, pp. 507–520, Mar. 2011, doi: 10.1109/TCSI.2010.2072430.

[16] F. Chen, A. P. Chandrakasan, and V. M. Stojanovic, "Design and analysis of a hardware-efficient compressed sensing architecture for data compression in wireless sensors," *IEEE J. Solid-State Circuits*, vol. 47, pp. 744–756, Mar. 2012, doi: 10.1109/JSSC.2011.2179451.

[17] K. Nagai, D. Kanemoto, and M. Ohki, "Applying K-SVD dictionary learning for EEG compressed sensing framework with outlier detection and independent component analysis," *IEICE Trans. Fundamentals*, vol. E104-A, no. 9, pp. 1375–1378, Sep. 2021, doi: 10.1587/transfun.2020EAL2123.

[18] M. Fira and L. Goras, "Comparison of inter- and intra-subject variability of P300 spelling dictionary in EEG compressed sensing," *Int. J. Adv. Comput. Sci. Appl.*, vol. 7, no. 10, pp. 366–371, Apr. 2016, doi: 10.14569/IJACSA.2016.071049.

[19] Y. C. Eldar, P. Kuppinger, and H. Bolcskei, "Block-sparse signals : uncertainty relations and efficient recovery," *IEEE Trans. Signal Process*, vol. 58, no. 6, pp. 3042–3054, Jun. 2010, doi: 10.1109/TSP.2010.2044837.

[20] A. Shoeb, "Application of machine learning to epileptic seizure onset detection and treatment," Ph.D. dissertation, Massachusetts Institute of Technology, Sep. 2009. [Online]. Available: https://dspace.mit.edu/handle/1721.1/54669

[21] Z. Zhang and B. D. Rao, "Extension of SBL algorithms for the recovery of block sparse signals with intra-block correlation," *IEEE Trans. Signal Process*, vol. 61, no. 8, pp. 2009–2015, Apr. 2013, doi: 10.1109/TSP.2013.2241055.

[22] T. Torfs, V. Leonov, R. F. Yazicioglu, P. Merken, C. V. Hoof, R. J. Vullers, and B. Gyselinckx, "Wearable autonomous wireless electroencephalography system fully powered by human body heat," *SENSORS*, pp. 1269–1272, Dec. 2008, doi: 10.1109/ICSENS.2008.4716675.

[23] A. Dementyev and J. R. Smith, "A wearable UHF RFID-based EEG system," in *Proc. IEEE Int. Conf. RFID*, Apr. 2013, pp. 1–7, doi: 10.1109/RFID.2013.6548128.